Mechanisms of European Summer Drying under Climate Change

ALEXANDRE TUEL[a] AND ELFATIH A. B. ELTAHIR[b]

[a] *Institute of Geography, Oeschger Centre for Climate Change Research, University of Bern, Bern, Switzerland*
[b] *Ralph M. Parsons Laboratory, Massachusetts Institute of Technology, Cambridge, Massachusetts*

(Manuscript received 17 December 2020, in final form 16 August 2021)

ABSTRACT: The geography of Europe as a continental landmass, located between the arid Sahara and the cold high latitudes (both are dry in terms of absolute humidity), dictates the reliance during summer of southern Europe (south of 45°N) on stored water from winter and spring, and of northwestern Europe on a small concentrated low-level moisture jet from the North Atlantic. In a recent study, we explained the projected winter precipitation decline over the Mediterranean under climate change as due to shifts in upper tropospheric stationary waves and to the regional-scale land–water warming contrast. Here, based on the analysis of observations and output from models from phase 5 of the Coupled Model Intercomparison Project, we expand this theory further, documenting how the winter precipitation decline expands into southern Europe during spring, dictated by similar dynamical mechanisms, depleting soil moisture and setting the stage for drier summers via soil moisture–precipitation feedbacks. Over northwestern Europe, an anomalous anticyclonic circulation west of the British Isles displaces the low-level moisture jet northward, limiting moisture supply, and reducing low-level relative humidity and rainfall. Finally, we discuss how this comprehensive perspective of European summer climate change can help us better understand the variations across model projections, and pave the way for their reduction.

KEYWORDS: Europe; Atmosphere-land interaction; Atmospheric circulation; Hydrologic cycle; Precipitation; Climate prediction

1. Introduction

A large majority of climate models have long projected drier summers over much of southern and western Europe under future climate scenarios (Rowell and Jones 2006; Seager et al. 2014; Brogli et al. 2019; Grillakis 2019), the result of intense surface warming and a widespread decrease in precipitation, most intense between 40° and 50°N (Fig. 1c). Such trends threaten to put significant stress on human health, water resources, and agriculture (Samaniego et al. 2018), particularly in the regions of southern Europe where precipitation will also decline during winter (Fig. 1a). While drying trends over Europe occur in the bigger context of widespread subtropical drying, they stand out by their magnitude, much larger than over any other region (Fig. 1d).

Projections of summer drying in Europe have thus attracted significant attention in the literature, notably in the context of the recent record-breaking heatwaves and droughts that the continent experienced (Stott et al. 2004; Fischer et al. 2007; Bador et al. 2016; Kew et al. 2019; Vautard et al. 2020). It is now understood that positive feedbacks between a decline in soil moisture, precipitation, and surface temperature play a major role in explaining the robustness of European summer trends (Schär et al. 2004; Rowell and Jones 2006; Seneviratne et al. 2006). As the surface warms, so does evapotranspirative demand, leading to reduced cloud cover and precipitation, and enhanced surface warming (Rowell and Jones 2006; Boé and Terray 2014). These feedbacks are largely triggered by decreases in precipitation during winter and spring over much of southern Europe, which increase soil moisture deficits at the beginning of summer (Vautard et al. 2007; Haarsma et al. 2009; Wang et al. 2011). Still, the mechanism triggering this initial drying is not fully understood, in particular what determines its spatial extent.

In addition, changes in the regional circulation, characterized by higher sea level pressure (SLP) over the Atlantic Ocean and northern Europe, are thought to contribute to the regional drying (Boé et al. 2009; Bladé et al. 2012; Belleflamme et al. 2015) by enhancing low-level moisture divergence over Europe (Seager et al. 2014) and shifting the North Atlantic jet poleward (Haarsma et al. 2015). The contribution of circulation trends appears to be limited to northwestern Europe (Rowell and Jones 2006; Belleflamme et al. 2015), where it may account for more than half of the precipitation decline and much of intermodel spread (Boé et al. 2009; Haarsma et al. 2015), although other results have suggested it may extend to most of the continent (Seager et al. 2014). As such, the relative importance of these circulation trends in explaining the projected drying along different latitudinal belts across Europe is not fully understood, and deserves further study. The projected SLP increase in the North Atlantic results from reduced rates of ocean surface warming in that region, linked to a weakening of the Atlantic meridional overturning circulation (AMOC) (Haarsma et al. 2015). Large-scale continent–ocean warming contrasts may also further depress land relative humidity through lesser rates of increase in evaporation above oceans (Byrne and O'Gorman 2018; Brogli et al. 2019).

A complex picture of European summer climate change thus emerges (Zappa 2019), in which several robust and

Supplemental information related to this paper is available at the Journals Online website: https://doi.org/10.1175/JCLI-D-20-0968.s1.

Corresponding author: Alexandre Tuel, alexandre.tuel@giub.unibe.ch

DOI: 10.1175/JCLI-D-20-0968.1

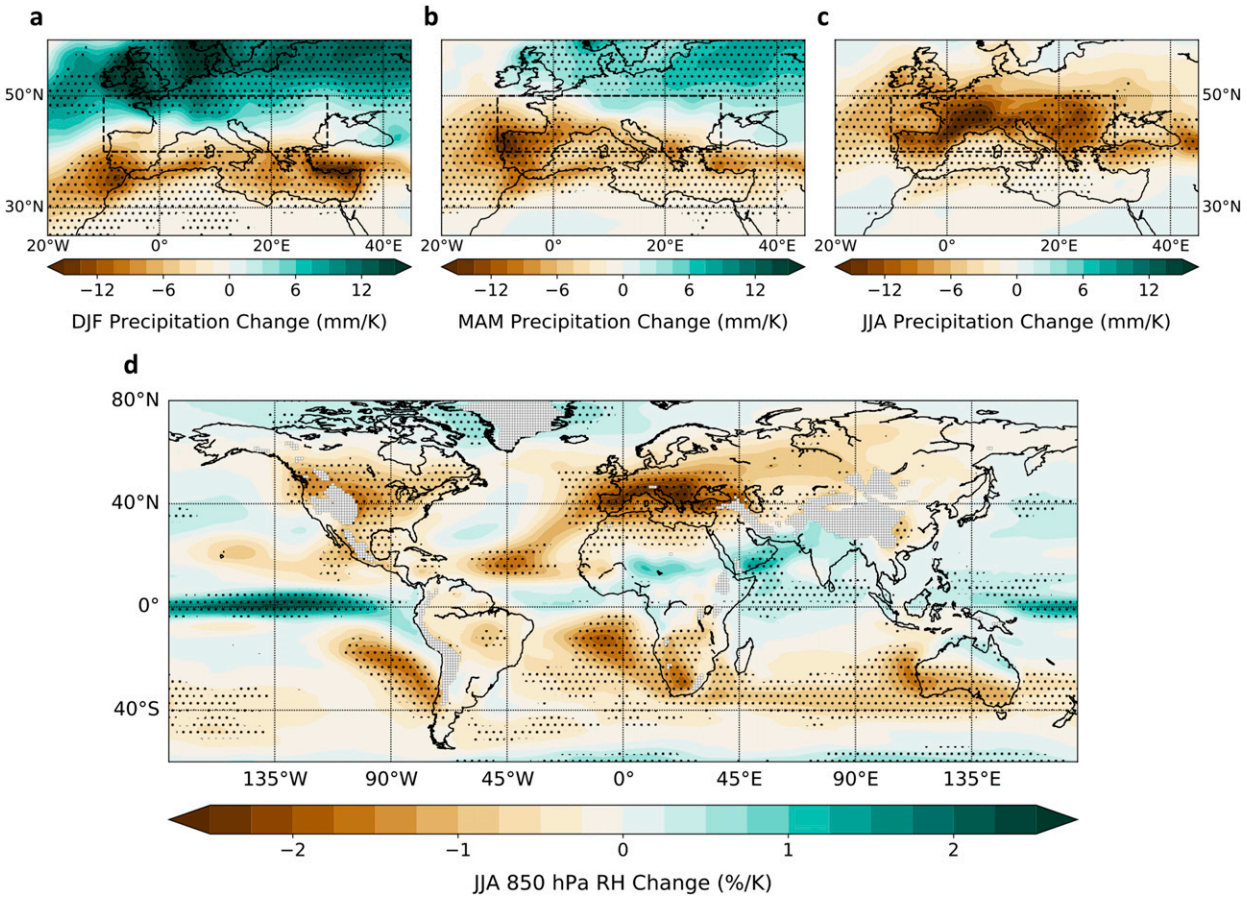

FIG. 1. CMIP5 multimodel mean change under RCP8.5 (2071–2100 minus 1976–2005) in European (a) DJF, (b) MAM, and (c) JJA precipitation, and in (d) global JJA 850-hPa relative humidity. Projections are normalized by each model's global-mean projected temperature change. Stippling indicates agreement by at least 80% of models on the sign of the change. Gray hatching in (d) covers areas where the 850-hPa level is below the surface.

well-understood physical mechanisms combine to bring hotter and more arid summers. Still, it remains unclear why the summertime European climate, in comparison to other geographical regions, would be particularly sensitive to soil moisture feedbacks and circulation changes. What makes the region so vulnerable, leading to such unparalleled drying trends in future projections? We provide an answer to this question by putting European summer drying trends in the context of the continent's current climate. First, we show why regions south of 45°N are vulnerable to changes in wet-season precipitation, and we demonstrate that mechanisms responsible for the projected winter precipitation decline in the Mediterranean also come into play during spring, expanding the precipitation decline northward into southern Europe and setting the stage for soil moisture depletion into summer. By investigating the detailed vertical structure and meridional distribution of the moisture inflow from the Atlantic, we also show that the summer climate north of 45°N is sensitive to trends in low-level moisture flux along the western coast of the continent. We conclude by offering a comprehensive picture of physical mechanisms of future European summer drying, and discuss their relevance to understand intermodel differences and reduce the associated uncertainty.

2. Data and methods

Our analysis focuses on a domain (hereafter referred to as the "European domain") that extends from 10°W to 30°E and from 40° to 50°N. The choice of this domain is based on the pattern of future precipitation projections (Fig. 1c): it covers most of the land area in Europe where models project a robust summer precipitation decline. We focus on three seasons: winter [December–February (DJF)], spring [March–May (MAM)], and summer [June–August (JJA)]. The reference for the current climate is ERA5 (Hersbach et al. 2020), the latest of the ECMWF reanalyses. ERA5 is based on an atmospheric model and reanalysis system with a horizontal grid spacing of about 31 km and is currently available over the 1979–2019 period. Using ERA5, we analyze specific humidity, relative humidity (RH), temperature, and winds archived on a regular 1° grid with 17 pressure levels, as well as precipitation (P) and evapotranspiration (E). Horizontal winds and specific

humidity are downloaded at a 6-hourly resolution to calculate time-mean horizontal moisture fluxes, while other variables are extracted at monthly resolution only. Because P in ERA5 is a prognostic variable (i.e., not directly assimilated), we also use observation-based P datasets at the monthly time scale: the Global Precipitation Climatology Project version 2.3 dataset (GPCP; 2.5° resolution) (Adler et al. 2003), and the two land-only datasets CRU TS4.04 (0.5° resolution) (Harris et al. 2020) and EOBS (0.25° resolution) (Cornes et al. 2018). Evaporation in ERA5 is also not assimilated, and thus is influenced by inevitable biases in precipitation and soil moisture data. Finally, soil moisture observations (top 1 m) are taken from the ESA CCI Soil Moisture v05.2 combined product (Gruber et al. 2019). Monthly-mean soil moisture values are calculated by averaging all nonmissing observations at each grid cell and for each available month. For purposes of comparison, we also analyze top 1-m soil moisture from ERA5.

Climate model output data from CMIP5 models (Taylor et al. 2012) are also analyzed, under the historical (1976–2005) and RCP8.5 (2071–2100) scenarios. We retained all 29 models that provided SLP, P, E, and RH at monthly resolution. For analyses involving moisture fluxes, we use a subset of 23 models for which horizontal wind and specific humidity data on pressure levels were available at daily resolution. Similarly, soil moisture data are only available for 19 of the 29 models. A detailed list of the selected models can be found in Table S1 in the online supplemental material (expansions of model acronyms are available at https://www.ametsoc.org/PubsAcronymList). All model output is bilinearly regridded to a common 1° × 1° grid, with land and ocean values regridded separately for surface/1000-hPa variables only. Future changes are defined under RCP8.5 with respect to the 1976–2005 historical average. We normalize them by each GCM's annual- and global-mean temperature change to remove, at first order, the effect of varying climate sensitivity across models. This is important to avoid overestimating intermodel correlations in long-term changes.

Given $q(p)$ the specific humidity (kg kg^{-1}) and $\mathbf{u}(p)$ the horizontal wind (m s^{-1}) at pressure p (Pa), at a 6-hourly (in ERA5) and daily (in CMIP5) resolution, we compute the seasonal-mean tropospheric moisture flux as the vertical integral of the seasonal-averaged moisture flux $\overline{q\mathbf{u}}$ between $p_0 = 1000$ and $p_1 = 100$ hPa:

$$\mathbf{F} = -\frac{1}{g}\int_{p_0}^{p_1} \overline{q\mathbf{u}}\, dp, \tag{1}$$

where $\bar{\cdot}$ stands for the seasonal average and $g = 9.81$ m s^{-2}. For the GCM simulations, we also define estimates of future summertime moisture fluxes under a "constant-wind-and-RH" assumption as follows. For each model, pressure level p and grid point, we note $\overline{\mathrm{rh}_{\mathrm{hist}}}$, the JJA-mean RH in the historical scenario; $\mathbf{u}_{\mathrm{hist}}(t)$ and $T_{\mathrm{hist}}(t)$, the daily horizontal wind and air temperature in the historical scenario; and $T_{\mathrm{RCP85}}(t)$, the daily air temperature in the RCP8.5 scenario. We first sort JJA-only daily T_{RCP85} values in the same order as those of JJA-only T_{hist}. This yields the series $T_{\mathrm{RCP85}}(t')$. Then, we calculate at time step t a future specific humidity value assuming no change in mean seasonal RH as follows:

$$\hat{q}_{\mathrm{RCP85}}(t) = \epsilon \frac{e_s[T_{\mathrm{RCP85}}(t')]}{p}\overline{\mathrm{rh}_{\mathrm{hist}}}, \tag{2}$$

where $e_s(T)$ is the saturation vapor pressure of water at temperature T and $\epsilon = 0.622$ is the molecular weight ratio of water vapor to dry air. The estimated horizontal moisture flux $\hat{\mathbf{F}}_{\mathrm{RCP85}}$ is then obtained by

$$\hat{\mathbf{F}}_{\mathrm{RCP85}} = -\frac{1}{g}\int_{p_0}^{p_1} \overline{\hat{q}_{\mathrm{RCP85}}\mathbf{u}_{\mathrm{hist}}}\, dp. \tag{3}$$

The seasonal atmospheric water budget for an atmospheric column above area $\mathscr{A}$ can then be written as

$$P - E = -\nabla \cdot \mathbf{F}, \tag{4}$$

with P, E, and $\mathbf{F}$ being the area-integrated seasonal-mean values of precipitation, evapotranspiration, and horizontal moisture flux respectively. The two moisture sources for the atmospheric column above area $\mathscr{A}$ are E and the incoming moisture flux F_{in}, defined as the horizontal advection of moisture into the column from all sides:

$$F_{\mathrm{in}} = \oint_{\partial\mathscr{A}} -\mathbf{F}\cdot\mathbf{n} \times 1(\mathbf{F}\cdot\mathbf{n} < 0), \tag{5}$$

where $\mathbf{n}$ is the unit vector normal to $\partial\mathscr{A}$. We use F_{in} to assess the role of horizontal moisture fluxes against that of E in the seasonal atmospheric moisture budget over the previously defined European domain. Finally, the seasonal surface water budget for area $\mathscr{A}$ is given by

$$P - E = \Delta W_s + R, \tag{6}$$

where ΔW_s is the area-integrated change in water storage and R the runoff flowing out of area $\mathscr{A}$.

As in Tuel and Eltahir (2020), to which we refer the reader for a more complete description of the methodology, we estimate the impact of upper-tropospheric (300 hPa) wind trends on Northern Hemisphere SLP during MAM with a dynamical adjustment technique based on constructed circulation analogs. For each GCM, analogs of each future MAM 300-hPa zonal wind anomaly field between 2071 and 2100 are identified in that model's historical run, and the corresponding SLP anomalies are linearly combined with optimal weights. The domain used to identify analogs and compute the weights is the latitude band extending from 15° to 65°N.

We also make use of the regional simulations developed by Tuel and Eltahir (2020) to assess the impact of reduced rates of warming of near-surface air above the Mediterranean Sea compared to surrounding continents. The simulations extend over a domain covering most of Europe and the Mediterranean Basin, spanning approximately 24°–53°N, 20°W–45°E, at a horizontal resolution of 35 km and using 40 vertical levels. They are run with the MIT Regional Climate Model (MRCM). MRCM is based on the Abdus Salam International Centre for Theoretical Physics Regional Climate Model, version 3 (RegCM3) (Pal et al. 2007) and includes several improvements achieved through incorporation of new physical schemes or

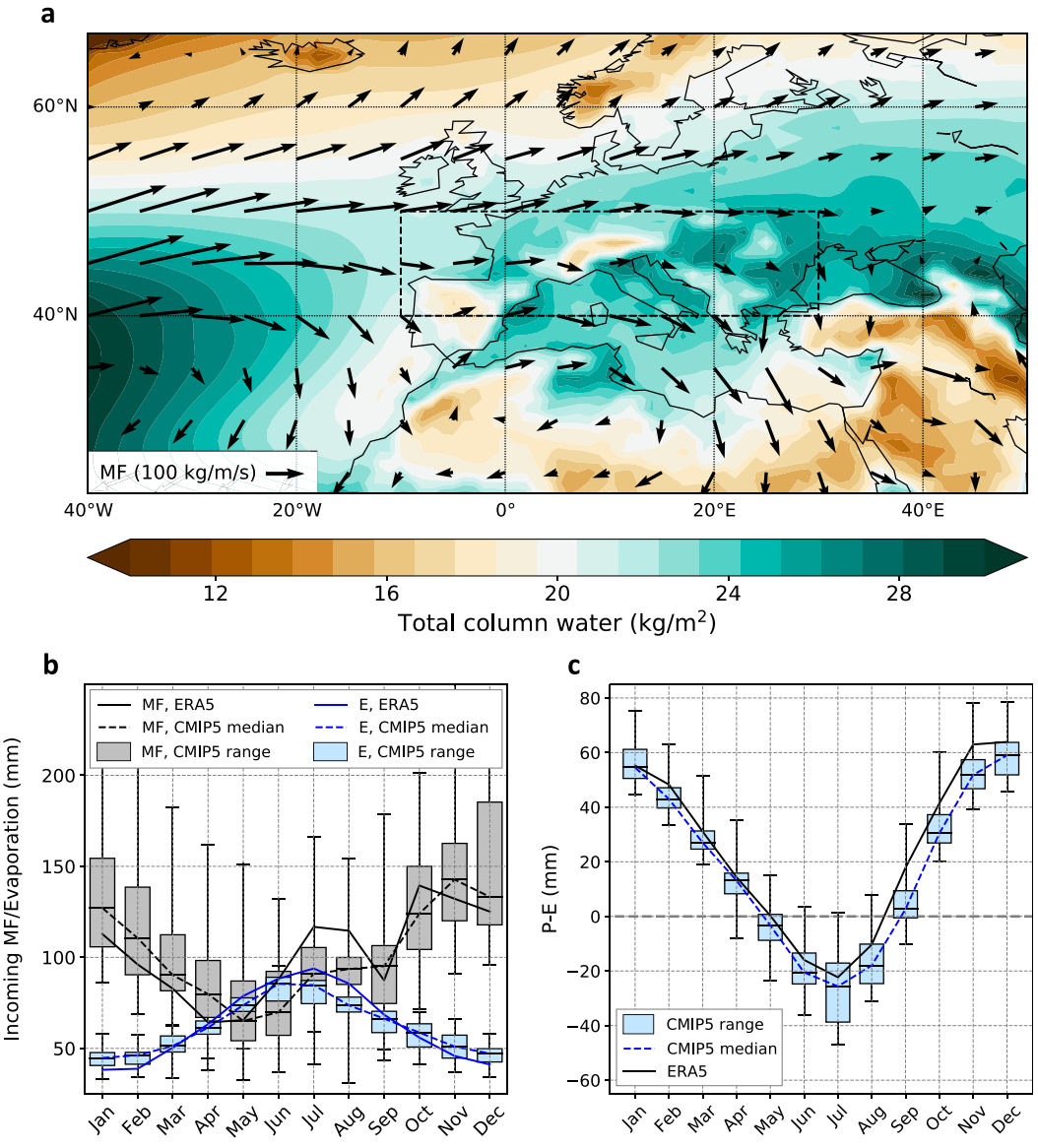

FIG. 2. (a) Column-integrated water (1000–100 hPa) (shaded) and horizontal moisture flux (arrows) over Europe during JJA, in the ERA5 reanalysis (1979–2019). (b) Annual cycle in incoming moisture flux F_{in} (black/gray shading) and surface (land + ocean) evaporation (blue) within the European domain (10°W–30°E, 40°–50°N), in ERA5 (solid lines) and across CMIP5 models (boxes and dashed lines). (c) Annual cycle in $P - E$ (land-only) over the European domain, in ERA5 (solid black) and across CMIP5 models (boxes; dashed blue line). In (b) and (c), whiskers extend over the full intermodel spread.

modification of original schemes [see Tuel and Eltahir (2020) and references therein]. Two sets of simulations were conducted (Im et al. 2014): one forced using ERA-Interim as boundary conditions over the 1981–2011 period, and one forced with output from the MPI-ESM-MR model under the RCP8.5 scenario between 2070 and 2100. Each set consists of a reference (unperturbed) experiment (designated by "0C") and a perturbed experiment in which Mediterranean SSTs are uniformly warmed by 1.5°C year-round (designated by "+1.5C"). The impact of the relative SST cooling on the regional climate can then be estimated by subtracting the results from the +1.5C simulation to those of the 0C simulation. The MPI experiments are intended to assess the impact of a relative Mediterranean cooling in a climate change context. Since any GCM presents a number of biases in its background climate, which may modulate the impact of the relative cooling, the ERA experiments thus allow us to assess the circulation impact of a relative cooling in the current Mediterranean climate with no land warming.

3. Europe's summer moisture budget in the current climate

To understand the large-scale historical context of summer drying projections over Europe, we begin by showing in Fig. 2a

tropospheric horizontal moisture fluxes and total column water (TCW) during the summer (JJA) season. The European domain stands out as a local TCW maximum, particularly its eastern part (the Balkans). TCW in regions to the north of the domain, poleward of 55°N, is about as low as over the Sahara Desert to the south (15–20 kg m^{-2}). To the west, over the Atlantic Ocean, TCW is also comparatively lower over an elongated coastal band between 20°W and 0°. The summer horizontal moisture flux is characterized by a narrow, westerly low-level jet extending between 45° and 55°N, and stretching from the North Atlantic into northern Europe, up to 20°–30°E. As a consequence, the incoming moisture flux into the European domain F_{in} is largely westerly, with the western border of the domain accounting for 80% of the magnitude of F_{in}.

How does Europe maintain its humidity under such conditions? On the one hand, atmospheric moisture fluxes advect moisture onto the continent, but mainly northward of 45°N (Seager et al. 2014). In addition, the moisture supply coming directly from surface (land and ocean) evapotranspiration E within the domain makes up a substantial fraction of incoming moisture into the lower troposphere (Fig. 2b). Note that E reaches its minimum in January and its maximum in July, and its share in the total moisture supply ($F_{in} + E$) goes from ~30% during winter to ~50% during summer, a phenomenon generally well reflected in CMIP5 models (Fig. 2b). In ERA5, F_{in} is about as large in summer as in winter, despite higher specific humidity, since the storm track is displaced poleward. In CMIP5 models, however, the summer F_{in} tends to be smaller than in winter, possibly a consequence of the zonal bias in the North Atlantic storm track in GCMs. The value of E is maximal during summer, even exceeding P, which leads to negative $P - E$ (Fig. 2c) from June to August. Negative $P - E$ can only be sustained by the depletion of soil and surface water storage [ΔW_s; Eq. (6)]. The latter is replenished from October to April, when P exceeds E.

The analysis of Fig. 2 concerns the European domain as a whole. However, the two halves of the domain (northern, from 45° to 50°N, and southern, from 40° to 45°N) behave differently (Figs. 3a,b). During summer, the northern half stands under the influence of the midlatitude storm track, which advects significant amounts of moisture and results in substantial P (its annual maximum is reached in June) (Fig. 3a). Consequently, while E is high, $P - E$ remains close to zero from June to August, and soil moisture in the ESA data hardly decreases. Still, ERA5 is in disagreement as it points toward a substantial soil moisture decline in the same period (down to −20 mm in June). Soil moisture increases again in September as $P - E$ becomes positive. By contrast, southward of 45°N, P drops during summer, just as E reaches its maximum (Fig. 3b). Thus $P - E$ is strongly negative from May to September, which leads to soil moisture depletion. ESA and ERA5 data are in agreement on the sign of soil moisture changes, but the magnitude is about twice as large in ERA5 as in ESA. Both datasets also agree that soil moisture changes during summer are more negative than in the northern half. Again, soil moisture increases from September onward, when $P - E$ becomes positive. This suggests that, south of 45°N, a larger fraction of summer E (and runoff) comes from soil moisture depletion compared to regions north of 45°N.

The relationship between winter/spring P, $P - E$, soil moisture anomalies, and summer evaporation also emerges in the analysis of interannual variability (Figs. 3c–e). While P in DJF is not significantly correlated to June soil moisture (Fig. 3c), it is for MAM in many parts of the European domain: the Iberian Peninsula, large parts of France, Italy, and the Balkans (Fig. 3d). May soil moisture anomalies in turn significantly impact JJA E over the same regions (Fig. 3e). Consequently, $P - E$ during spring (and to a lesser extent winter), which replenishes soil moisture levels before the summer, is positively correlated to summer 850-hPa RH over much of the southern half of the European domain (Fig. 4a; see also Fig. S1 in the online supplemental material). Poleward of 45°N, the connection between winter and summer conditions appears reversed, though not significant. A similar pattern is also present in observation-based P datasets (Figs. 4c,d) but with weaker magnitude and no statistical significance, which might be due to the fact that P is less relevant than $P - E$ for the soil moisture budget. The correlations between spring $P - E$ summer and 850-hPa RH are significant over much of the Iberian Peninsula and locally over the Balkans, regions where summer E is most reliant on soil moisture accumulated during the cold season. While correlation significance is limited in observations, CMIP5 models reproduce the overall correlation pattern over southern Europe, with strong intermodel agreement over the Iberian Peninsula and the Balkans (Fig. 4b). This increases our confidence in the physical interpretation of the observation-based correlations.

During summer, the European domain is therefore dependent on wet-season water storage and on the narrow low-level Atlantic moisture jet to maintain its humidity. As such, any change in either of these moisture sources driven by climate change can impact summer moisture availability over Europe and, consequently, precipitation. Based on this perspective, we consider in the following each moisture source in turn, look at its projected trends under future climate scenarios, and explain how these trends contribute to projections of summer drying over Europe.

4. Wet season precipitation decline and impact on European summer climate

a. Changes in the surface water balance: Winter, spring, and summer

Climate models have long projected a significant decline in precipitation during winter and spring over southern Europe and the Mediterranean Basin (Seager et al. 2014; Lionello and Scarascia 2018). In winter, absolute changes are most negative over northwestern Africa, the southern Iberian Peninsula, and along the eastern Mediterranean coastline (Tuel and Eltahir 2020), whereas over northern Europe precipitation is expected to increase substantially (Fig. 1a). During spring, the decline in precipitation shifts northward into southern Europe, extending up to 45°N, while from 45° to 50°N precipitation is projected to remain roughly constant (Fig. 1b). These patterns are reflected in $P - E$ projections. During winter, the $P - E$ decline is essentially limited to the Mediterranean coastline, and is robust

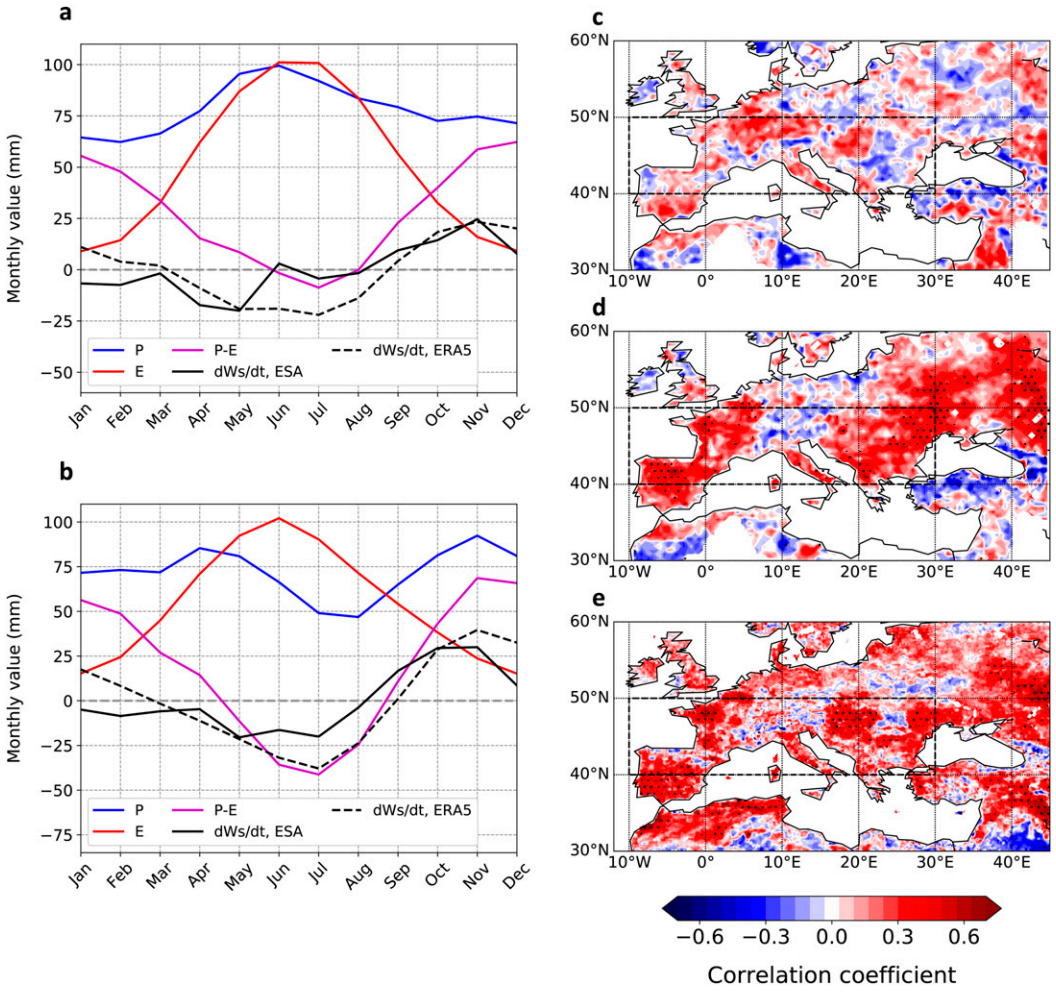

FIG. 3. (a) Annual cycle in land-only P (blue), E (red), $P - E$ (purple), and monthly soil moisture changes (black) for the southern half of the European domain (10°W–30°E, 40°–45°N). All data are from ERA5 except soil moisture (solid black) from the ESA dataset. (b) As in (a), but for the northern half of the domain (10°W–30°E, 45°–50°N). Pointwise correlation coefficient between (c) DJF and (d) MAM P (from EOBS dataset) and June soil moisture (from ESA dataset). (e) Pointwise correlation coefficient between May soil moisture (from ESA dataset) and JJA E (from ERA5). Stippling in (c)–(e) indicates significance at the 10% level, after correcting for the false discovery rate according to Wilks (2016).

in the southern half of our domain (Fig. 5a). During spring, it extends northward into western and central Europe, up to 50°N (Fig. 5b). In summer, the decline progresses farther northward: it is mainly concentrated at latitudes higher than 45°N, while $P - E$ is projected to remain constant, or even to increase slightly, in the regions to the south (Fig. 5c).

In winter and spring, the projected decreases in $P - E$ over the western half of the European domain (the Iberian Peninsula and Italy in DJF/MAM, France in MAM) are mainly driven by negative P trends, since projections show relatively constant or increasing E in these regions (Figs. 5d,e). In the eastern half, however (the Balkans), the P decline is mostly restricted to Greece; higher north it is the increase in E that explains the negative $P - E$ trend. In summer, the P decline between 40° and 45°N is roughly compensated by a decline in E, which is particularly strong over the Balkans and the Iberian Peninsula (Fig. 5f), leading to the weak $P - E$ trends of Fig. 5c. By contrast, E remains relatively unchanged north of 45°N, and it is the decrease in P that explains the negative $P - E$ change. In terms of soil moisture, changes within our domain are mainly negative (Figs. 5g–i). Large year-round declines are projected for the Iberian Peninsula and the Balkans. For the rest of the domain, the decline mainly occurs during summer, in parallel with that in $P - E$ (Fig. 5c). Soil moisture trends during winter and spring, though less robust, also point to a slight decline as well, despite $P - E$ remaining about constant there (Fig. 5a), a likely consequence of the summer decline whose impact is felt throughout the year.

b. *Mechanisms of spring precipitation and $P - E$ change*

The robust precipitation decline during winter, centered over the southwestern and eastern Mediterranean, is the result

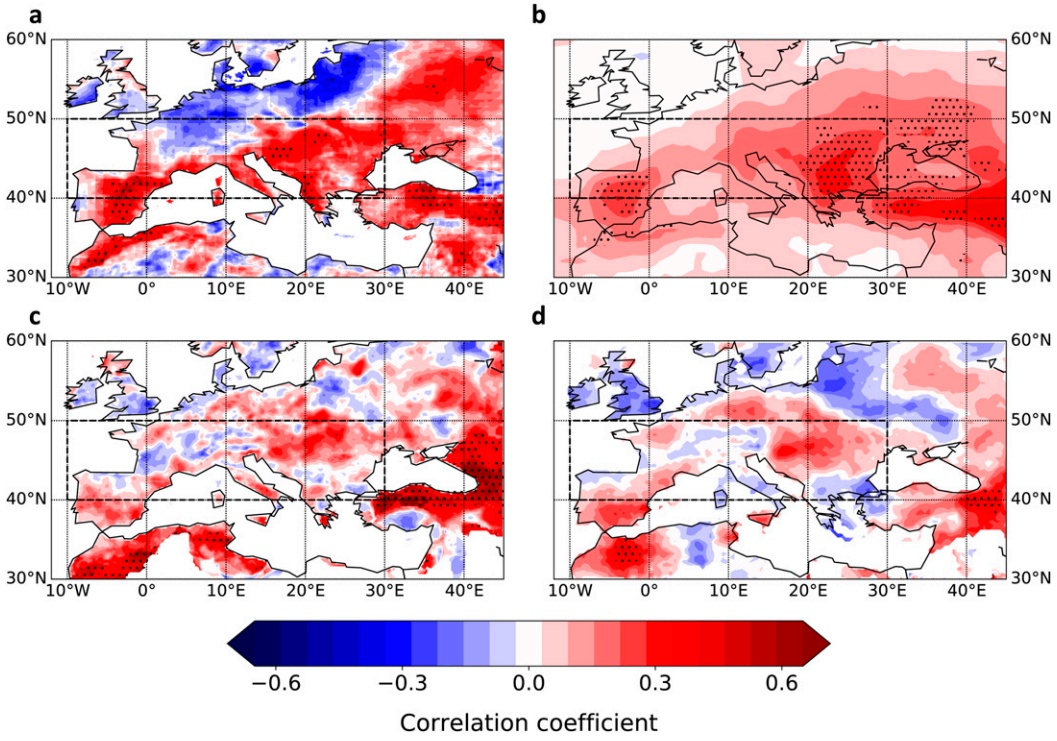

FIG. 4. (a) Pointwise correlation coefficient between December–May $P - E$ and JJA 850-hPa relative humidity (ERA5 data, 1979–2019). (b) CMIP5 multimodel mean pointwise correlation between December–May $P - E$ and JJA 850-hPa relative humidity, in the historical (1976–2005) simulations. Pointwise correlation coefficient between December–May P in (c) EOBS and (d) CRU, and JJA 850-hPa relative humidity in ERA5 (1979–2019). Stippling in (b) indicates agreement between at least 80% of CMIP5 models on the sign of the correlation, and in all other panels indicates significance of the correlation at the 10% level, after correcting for the false discovery rate according to Wilks (2016).

of an increase in average SLP over the Mediterranean Basin (Seager et al. 2014; Tuel and Eltahir 2020). Higher Mediterranean SLP indeed drives anomalous northerlies and the associated cold (and dry) advection over the eastern Mediterranean, which, following the energy balance, triggers adiabatic warming and a reduction in precipitation through anomalous subsidence. To the west, the SLP anomaly generates anomalous dry advection from the Sahara Desert toward Morocco and the southern Iberian Peninsula, in addition to weakening the Atlantic moisture supply, which reduces RH in the lower troposphere and decreases convective instability (Tuel et al. 2021a). The pronounced SLP increase is itself a response to shifts in the upper-tropospheric planetary circulation and to the regional-scale warming contrast between the Mediterranean and surrounding land (Tuel and Eltahir 2020). The strengthening of upper-tropospheric zonal winds, linked to enhanced warming at upper levels in the tropical troposphere, lengthens the wavelength of stationary planetary waves (Simpson et al. 2016; Wills et al. 2019). This leads to a robust anticyclonic anomaly over the Mediterranean, which, due to zonal asymmetries in the vertical structure of stationary waves, is transmitted down to the surface with limited dampening (Tuel et al. 2021b). Additionally, the surface heating anomaly due to reduced rates of warming of Mediterranean SSTs compared to land also leads to higher SLP over the basin.

During spring, southern Europe and the Mediterranean are also characterized by significant positive SLP trends and associated anticyclonic circulation (Fig. 6a). While winter trends are characterized by a strong anomalous ridge over the Mediterranean, European SLP trends during spring are weaker (roughly 1 hPa compared to 2 hPa) and displaced to the west, where they connect with an area of robust enhanced SLP over the North Atlantic. Still, as is the case during winter (Tuel and Eltahir 2020), southern European and Mediterranean precipitation trends across CMIP5 models are primarily connected to SLP changes over southern Europe (southward of 45°N), and not over northwestern Europe and the Atlantic Ocean (Fig. 6b; see also Fig. S2), even though the latter are also robust. The relationship between spring Mediterranean (10°W–40°E, 35°–45°N) precipitation projections and the SLP increase over southern France and Italy in particular is very strong and explains half of intermodel scatter in precipitation projections ($r^2 = 0.55$). The reason, as in winter, can be found in the circulation anomaly triggered by such SLP trends. The robust SLP increase centered around 40°N, 10°E generates a substantial anticyclonic anomaly associated with anomalous southeasterlies and dry advection over southwestern Europe (Fig. 6c), and anomalous northerlies, cold and dry advection, as well as subsidence, over southeastern Europe and Turkey (Fig. 6d).

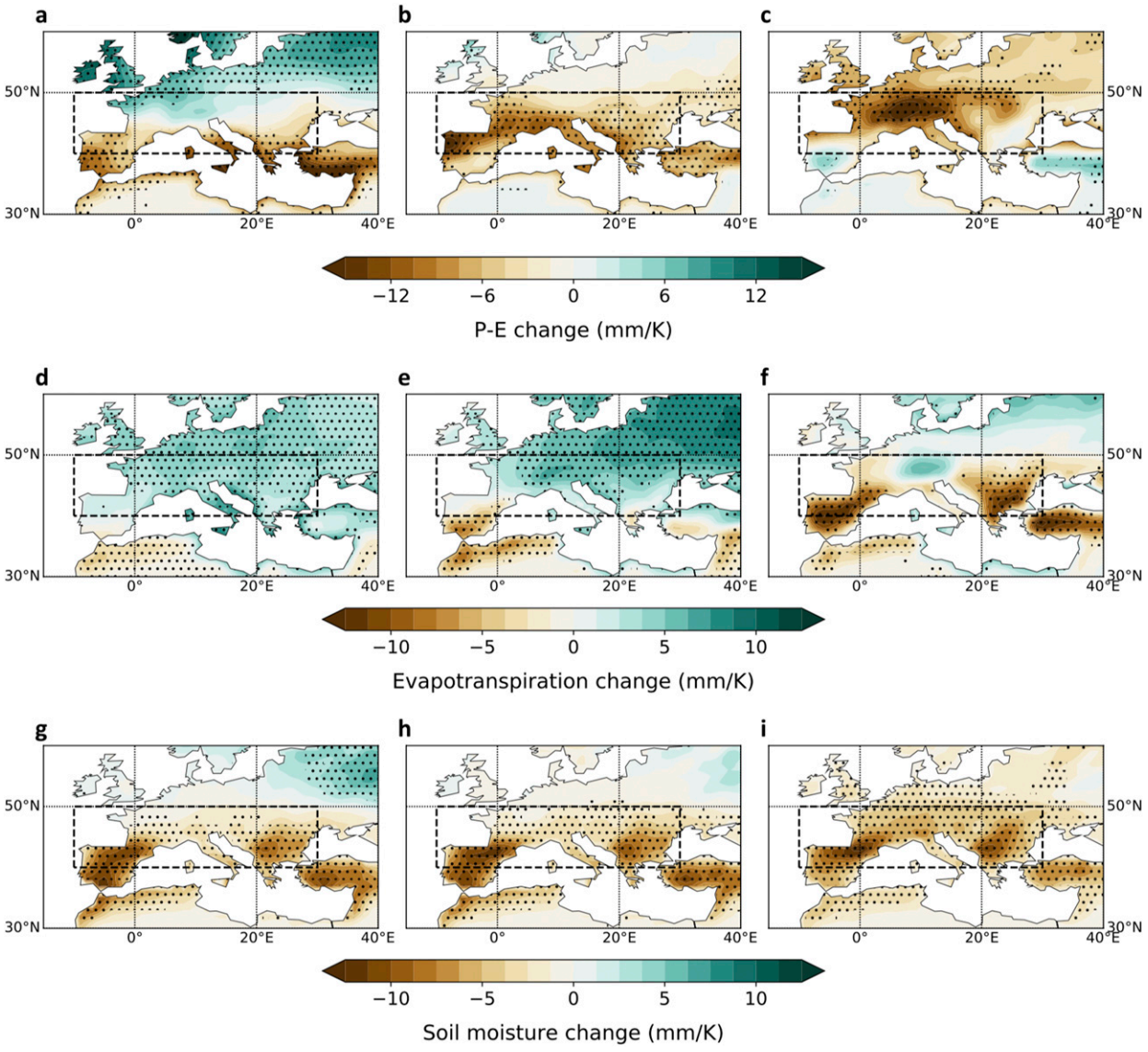

FIG. 5. CMIP5 multimodel mean change (2071–2100 minus 1976–2005) in (a)–(c) $P - E$, (d)–(f) E, and (g)–(i) soil moisture (top 1 m) over Europe (land only), in (left) DJF, (center) MAM, and (right) JJA. Stippling indicates agreement by at least 80% of models on the sign of the change.

Comparing spring (Fig. 6) to winter (Fig. S3), the P and $P - E$ declines shift northward during spring, particularly over the western Mediterranean. This shift is partly related to a similar northward drift of the anomalous SLP ridge from the central to the northwestern Mediterranean (Fig. 6a). Anomalous SLP gradients over the western Mediterranean are weaker during spring, but low-level wind trends are of a similar magnitude to those projected for winter (1–1.5 m s^{-1}). In addition, the projected low-level RH decline is stronger than during winter (Fig. 6c; see also Fig. S3c). This may result from the fact that the humidity difference (both absolute and relative) between the Sahara Desert and the Iberian Peninsula is larger during spring, and also from the storm track and associated moisture transport being more poleward during spring.

To the east, anomalous subsidence trends are noticeably weaker in MAM than in DJF, possibly a consequence of precipitation being smaller in this region during spring. Indeed, lower precipitation means less latent heating of the atmospheric column, which limits the possibility for reduced precipitation to enhance the subsidence signal through diabatic cooling feedbacks (Rodwell and Hoskins 2001). The location of enhanced subsidence is not significantly different in spring compared to winter, and in both seasons the precipitation decline remains centered over Greece and Turkey while regions around the Black Sea see little change in precipitation during either season (Figs. 1a,b). The $P - E$ decline expands northward during spring, however (Fig. 5b), driven by an increase in E.

c. *Origins of spring SLP trends*

The SLP increase over continental Europe is therefore the key driver of the projected P decline south of 45°N during

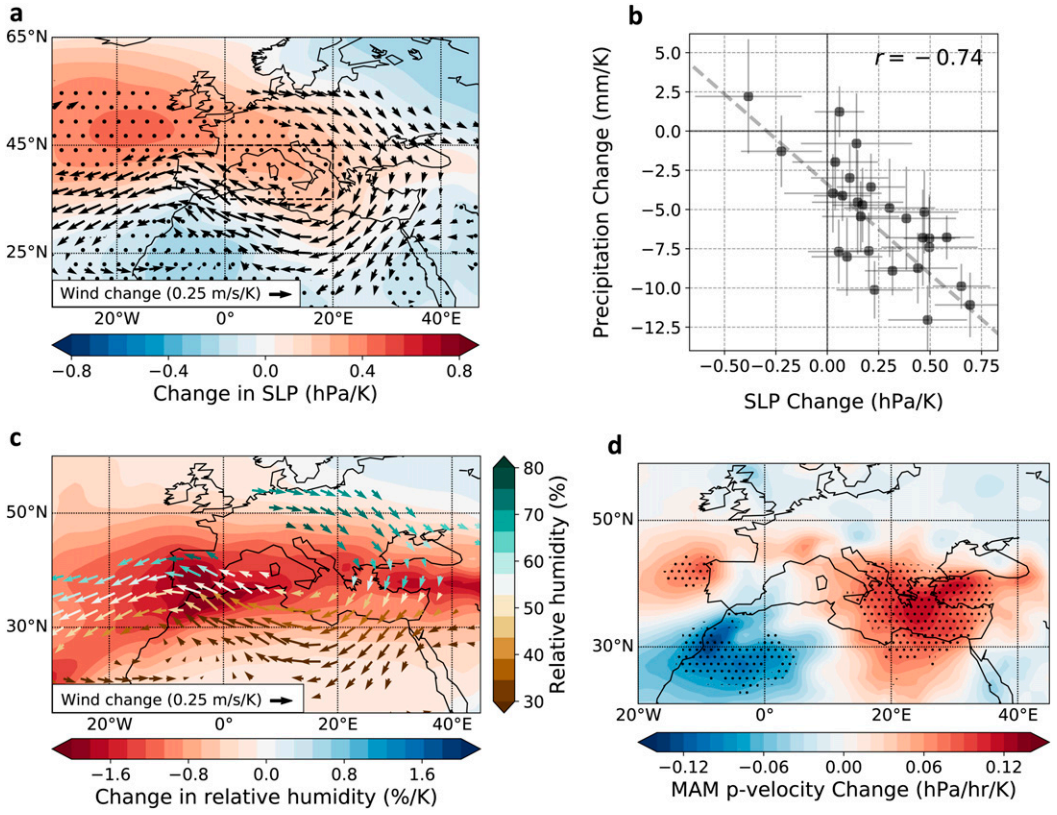

FIG. 6. (a) CMIP5 multimodel mean change (2071–2100 minus 1976–2005) in MAM SLP (shaded) and 850-hPa winds (arrows). (b) Change in MAM Mediterranean (10°W–40°E, 35°–45°N) precipitation and SLP [0°–20°E, 35°–45°N; see box in (a)] across CMIP5 models, with 95% confidence intervals and least squares best fit. (c) CMIP5 multimodel mean change in MAM 850-hPa relative humidity (shaded) and 850-hPa winds (arrows), where wind arrows are colored according to mean historical relative humidity at each point. (d) CMIP5 multimodel mean change in MAM 500-hPa pressure velocity. In (a) and (d) stippling indicates agreement by at least 80% of models on the sign of the change. In all panels changes are taken under the RCP8.5 scenario and are normalized by each model's global-mean projected temperature change.

spring, itself a major contributor to the concurrent $P - E$ decline over the same region (and beyond, over southern and eastern Europe). To understand what drives springtime SLP trends, and in particular whether similar mechanisms are at play as during winter, we first show in Figs. 7a and 7b the upper- and lower-tropospheric meridional wind trends projected for MAM by the CMIP5 multimodel ensemble. As in winter, a clear anticyclonic anomaly occurs right above the Mediterranean Basin, but of a magnitude about two-thirds that projected for winter (Tuel et al. 2021b). Near the surface, the anomalous northerly wind component is evident east of 20°E. The empirical approach of dynamical adjustment reveals that, similar to winter, upper-tropospheric dynamical trends during spring are linked to positive SLP anomalies over much of the Mediterranean Basin, particularly its western half, accounting for about half the projected CMIP5 multimodel trend over the 35°–45°N, 0°–20°E domain (+0.12 against +0.23 hPa K^{-1}; Figs. 7c,d). Compared to DJF, estimated SLP anomalies during MAM are shifted northwestwards, extending into southern France, consistent with projected upper-tropospheric circulation changes (Fig. S4). This shift between winter and spring is likely due to the concurrent poleward drift and weakening of the upper-tropospheric jet.

In spring, Mediterranean SSTs also experience a relative cooling with respect to the surrounding continents, due to the reduced rate of warming of ocean temperatures compared to land (Sutton et al. 2007). Its impact on the regional circulation, as estimated by the difference between the 0C and +1.5C MRCM experiments, is a basinwide SLP increase, reaching a maximum of 0.75 hPa over the central Mediterranean (20°E), and averaging +0.5 hPa over the previously defined southern European domain (35°–45°N/0°–20°E) (Fig. 8a). The wind response is essentially confined to the southeastern and southern Mediterranean, with very weak changes over southwestern Europe ($\leq 0.1\ m\ s^{-1}$). It is also associated with a broad decrease in precipitation (Fig. 8b), mostly eastward of 10°E, extending into the Balkans, where it amounts to about 10% of seasonal precipitation. In keeping with the previous discussion, very little difference in precipitation is seen over southern France and the Iberian Peninsula, where winds are roughly the same in the perturbed and unperturbed experiments.

Overall, the two mechanisms seem to explain most of the SLP change projected by CMIP5 models over southern

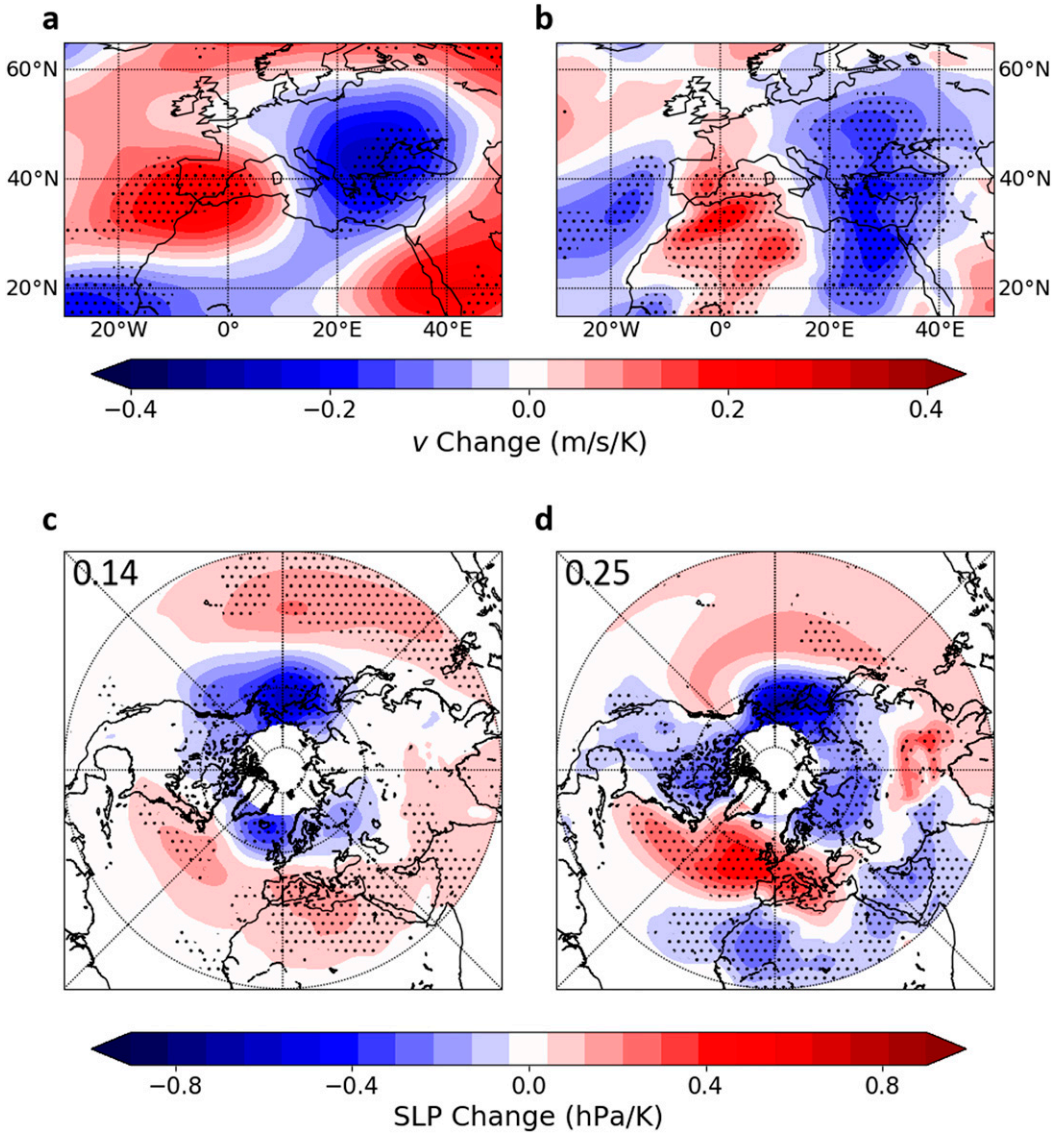

FIG. 7. CMIP5 multimodel mean change (2071–2100 minus 1976–2005) in (a) 300- and (b) 850-hPa MAM meridional winds over Europe. Also shown is Northern Hemisphere CMIP5 multimodel mean change in MAM SLP (c) estimated by dynamical adjustment and (d) projected by CMIP5 models. Numbers indicate average values within the 0°–20°E, 35°–45°N domain. In all panels stippling indicates agreement on the sign of the change by at least 80% of models.

Europe. Compared to winter, the spring SLP anomalies linked to each mechanism appear to be displaced westward (Tuel and Eltahir 2020), consistent with CMIP5 projections. It is important to note that neither mechanism can account for the robust SLP increase projected west of France and the British Isles (Fig. 6a). This positive SLP anomaly is generally thought to be the response to reduced SST warming over the North Atlantic (Haarsma et al. 2015; Gervais et al. 2019). While this SLP feature is not expected to have much influence over southern European and Mediterranean precipitation trends during spring, it may still matter by preventing the strengthening of midlatitude westerlies over northwestern Europe that would be expected from the SLP anomalies from Figs. 7c and 8a. Indeed, Fig. 6a shows the lack of a robust wind response over northwestern Europe, an important difference with winter projections (Tuel and Eltahir 2020). In winter, a strengthening in westerlies and in the associated moisture transport likely contributes to the large increase of precipitation projected for northern Europe, down to 50°N. Its absence during spring may therefore be linked to the much weaker and less robust precipitation signal over northern Europe, contributing to the overall stagnation in $P - E$ trends (Fig. 5b).

5. Moisture flux changes and impact on European summer moisture

a. *Analysis of projected moisture flux trends*

Atmospheric circulation changes during winter and spring lead to decreases in P and $P - E$ south of 45°N within the

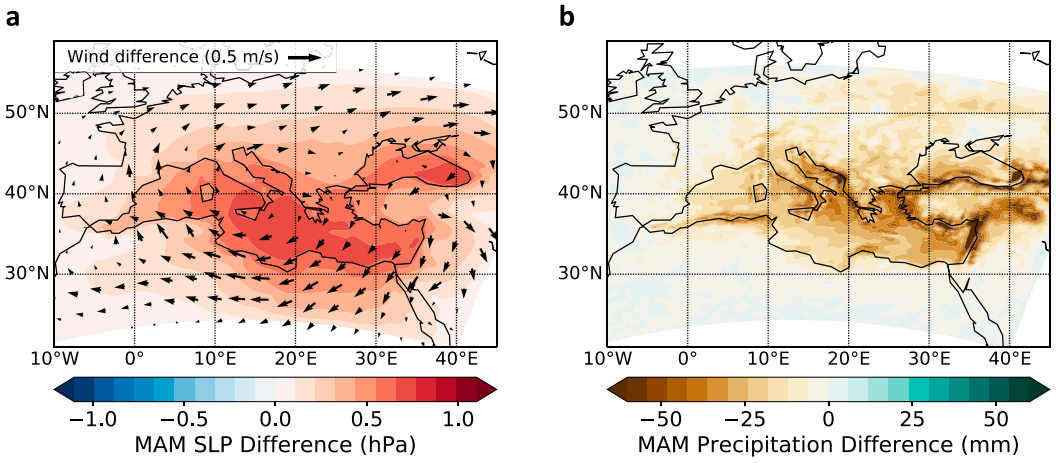

FIG. 8. Difference in MAM (a) SLP and 850-hPa winds and (b) precipitation, between the 0C and +1.5C simulations (0C minus +1.5C, average of ERA and MPI runs).

domain, setting the stage for a summertime P decline through soil moisture–rainfall feedbacks. North of 45°N, however, winter and spring trends in $P - E$ are weak (Figs. 5a,b), while summer P and low-level RH still exhibit sharp negative trends (Figs. 1c,d). In addition, summer E remains approximatively constant in future projections (Fig. 5f), which is inconsistent with a strong role for land–atmosphere coupling in the P decline. To understand summer P and RH trends, we analyze future horizontal moisture fluxes, particularly along the western border of the European domain (10°W, between 40° and 50°N), where the majority of moisture advection into the domain occurs (Fig. 2a). The vertically integrated moisture flux increases on average in future projections, leading to enhanced zonal moisture advection into Europe (Fig. 9a). However, we find, first, that the moisture flux increase along the western border of the domain is lower than what would be expected under an assumption of fixed circulation and RH (Fig. 9a) and, second, that at low levels (below 800 hPa) the zonal moisture flux along that same border even decreases in absolute terms (Fig. 9c), although the trend is not robust southward of 45°N. Northward of 60°N, by contrast, zonal moisture fluxes increase across the depth of the troposphere, slightly beyond the fixed-circulation/fixed-RH estimates (Fig. 9).

The weak increase in vertically integrated zonal moisture advection has direct implications for the summertime moisture budget over the European domain. Over the northern half of the European domain (see box in Fig. 9a), where we expect moisture flux trends to matter most for changes in the moisture budget, 850-hPa RH trends are found to be significantly connected to changes in vertically integrated zonal moisture inflow at 10°W ($r^2 = 0.3$; Fig. 9b). The correlation is even stronger when restricting the moisture flux to the 1000–600-hPa layer ($r^2 = 0.5$). Intermodel spread in projections remains large, however; six GCMs (a fourth of analyzed models) even project an absolute decline in vertically integrated zonal moisture inflow at 10°W.

Figure 10 shows 850-hPa RH and moisture flux projections for the six models with the most positive (Figs. 10a,b) and the most negative (Figs. 10c,d) moisture flux change in Fig. 9b. Clearly, the outlook for regions north of 50°N is very different between these two groups of models (Fig. 10e). Southern Europe (including the southern half of our domain, below 45°N), on the other hand, experiences sharp drying in either case, particularly over the Iberian Peninsula, the Balkans, and Turkey. These are precisely the regions where our previous results suggest that land–atmosphere coupling dominates both for interannual and long-term climate variability. The difference in RH trends between the two model groups confirms that uncertainties in moisture flux changes play only a limited role in RH projections (Fig. 10e).

b. *Role of dynamical trends*

Future moisture flux trends are determined by changes in specific humidity and circulation. The fact that zonal moisture fluxes between 40° and 50°N increase less than expected, assuming fixed circulation and RH, implies a decline in RH and/or a change in atmospheric circulation. Though robustly negative, RH trends west of 10°W are weak (Fig. 1d). Thus, while they undoubtedly contribute to the decline in zonal moisture fluxes relative to the ''fixed-circulation, fixed-RH'' baseline, they are unlikely to fully account for it. It is also unclear to what extent the RH decline west of 10°W is related to the concurrent decline over the European continent. Low-level circulation trends, on the other hand, clearly show anomalous easterlies over the 30°W–0°, 40°–45°N domain—where zonal moisture fluxes are projected to decline (Fig. 9c)—and anomalous westerlies northward of 55°N (Fig. 11a). Both are linked to positive SLP anomalies west of the British Isles, around 50°N, 20°W. An area of robust SLP decline also extends over the whole Mediterranean Basin and northern Africa, and it strengthens the anomalous SLP gradient over western Europe, thus enhancing the circulation response. Overall, uncertainties in moisture flux projections are linked to the magnitude of this SLP gradient. GCMs projecting an absolute decline in zonal moisture advection

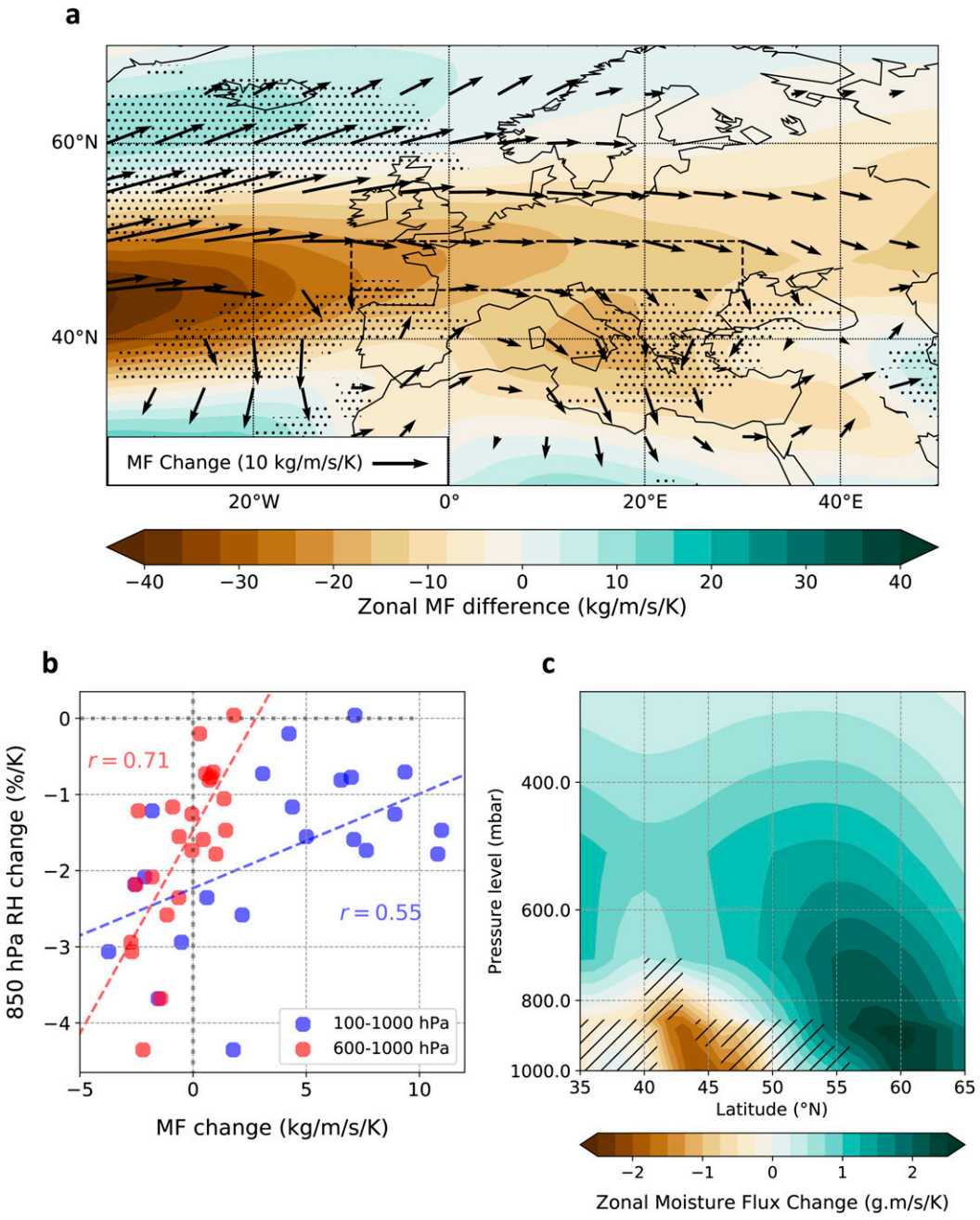

FIG. 9. (a) CMIP5 multimodel mean change (2071–2100 minus 1976–2005) in JJA vertically integrated (1000–100 hPa) horizontal moisture flux (arrows), and mean difference between the projected change in zonal moisture flux and the corresponding ''constant-wind-and-RH'' estimates (see section 2) (shaded). (b) JJA change across CMIP5 models in western European vertically integrated [1000–100 hPa (blue) and 1000–600 hPa (red)] zonal moisture flux at 10°W, averaged between 45° and 50°N, against projected change in 850-hPa RH over the 10°W–30°E, 45°–50°N domain [see box in (a)]. (c) CMIP5 multimodel mean change in JJA zonal moisture flux at 10°W on pressure levels. Dashed lines in (c) indicate lack of agreement on the sign of the change by at least 80% of models.

(Fig. 9b) also project a larger-than-average SLP increase from the North Atlantic to Scandinavia, and larger-than-average decrease over continental Europe (Fig. 11b). Results are opposite for the GCMs in which zonal moisture flux trends are most positive (Fig. 11c). Interestingly, the difference between these two groups of models is not largest in the area of robust multimodel SLP increase west of the British Isles. The spread in moisture flux trends is therefore

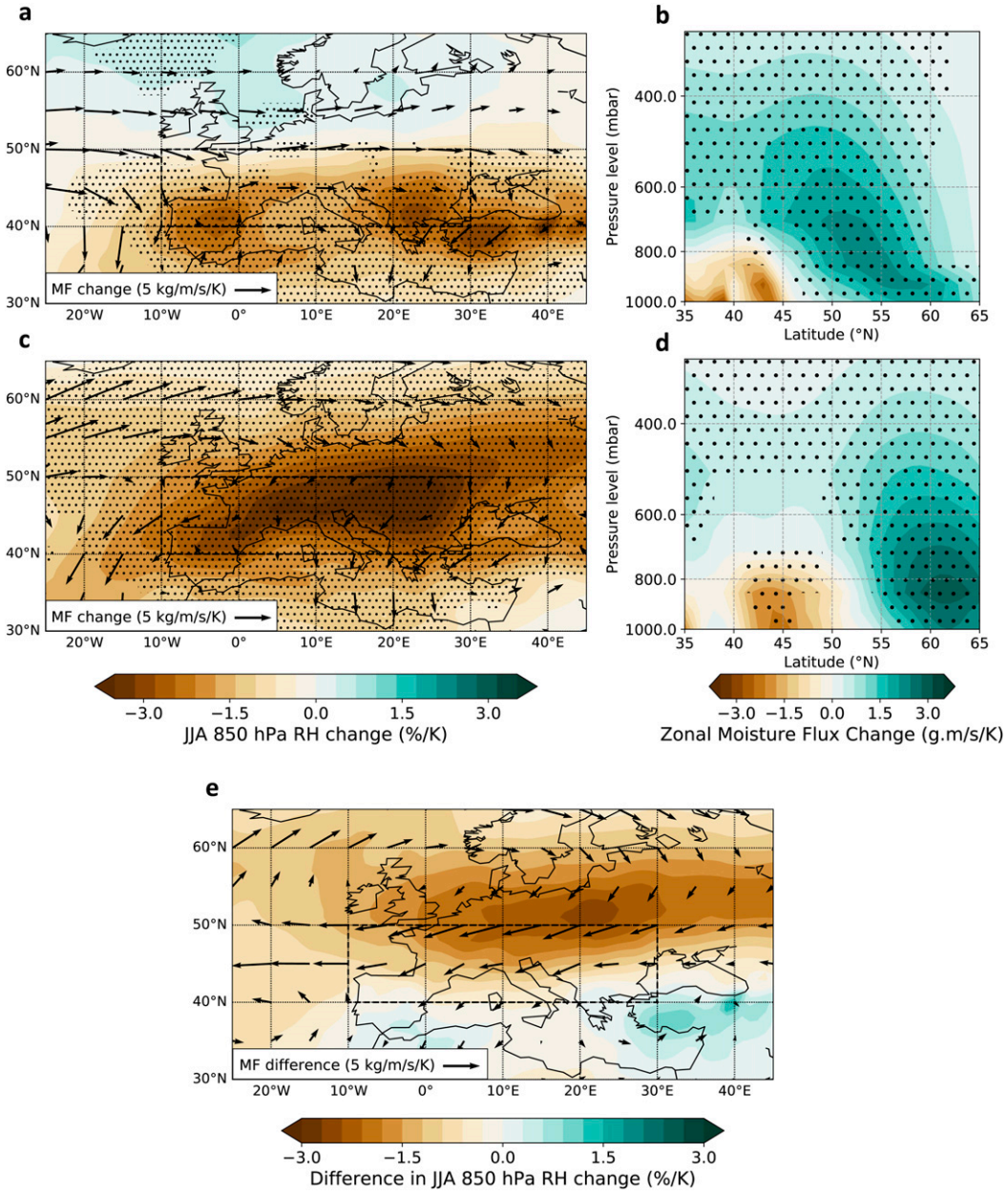

FIG. 10. Change in JJA (a) mean 850-hPa RH (shaded) and 925–600-hPa moisture flux (arrows), and (b) zonal moisture flux averaged between 10°W–0°, for the six CMIP5 models with the most positive moisture flux change in Fig. 9b. (c),(d) As in (a) and (b), but for the six models with the most negative moisture flux change. (e) Difference between (c) and (a). In (a)–(d), stippling indicates agreement on the sign of the change by all the models of the respective group.

related both to the magnitude and the pattern of future JJA SLP changes.

6. Discussion

Results from the present study confirm the complexity behind summer drying projections over Europe, but also suggest a comprehensive understanding of the physical mechanisms responsible, as shown in Fig. 12. In keeping with Brogli et al. (2019), our results suggest a prominent role for the land–ocean warming contrast, specifically the reduced North Atlantic warming, although primarily through its impact on regional circulation rather than through thermodynamics exclusively. Indeed, like Haarsma et al. (2015), we find a critical influence of North Atlantic SLP trends on northern European precipitation, which we interpret through their impact on incoming moisture fluxes into Europe. However, we argue also for an important effect from the Mediterranean heat

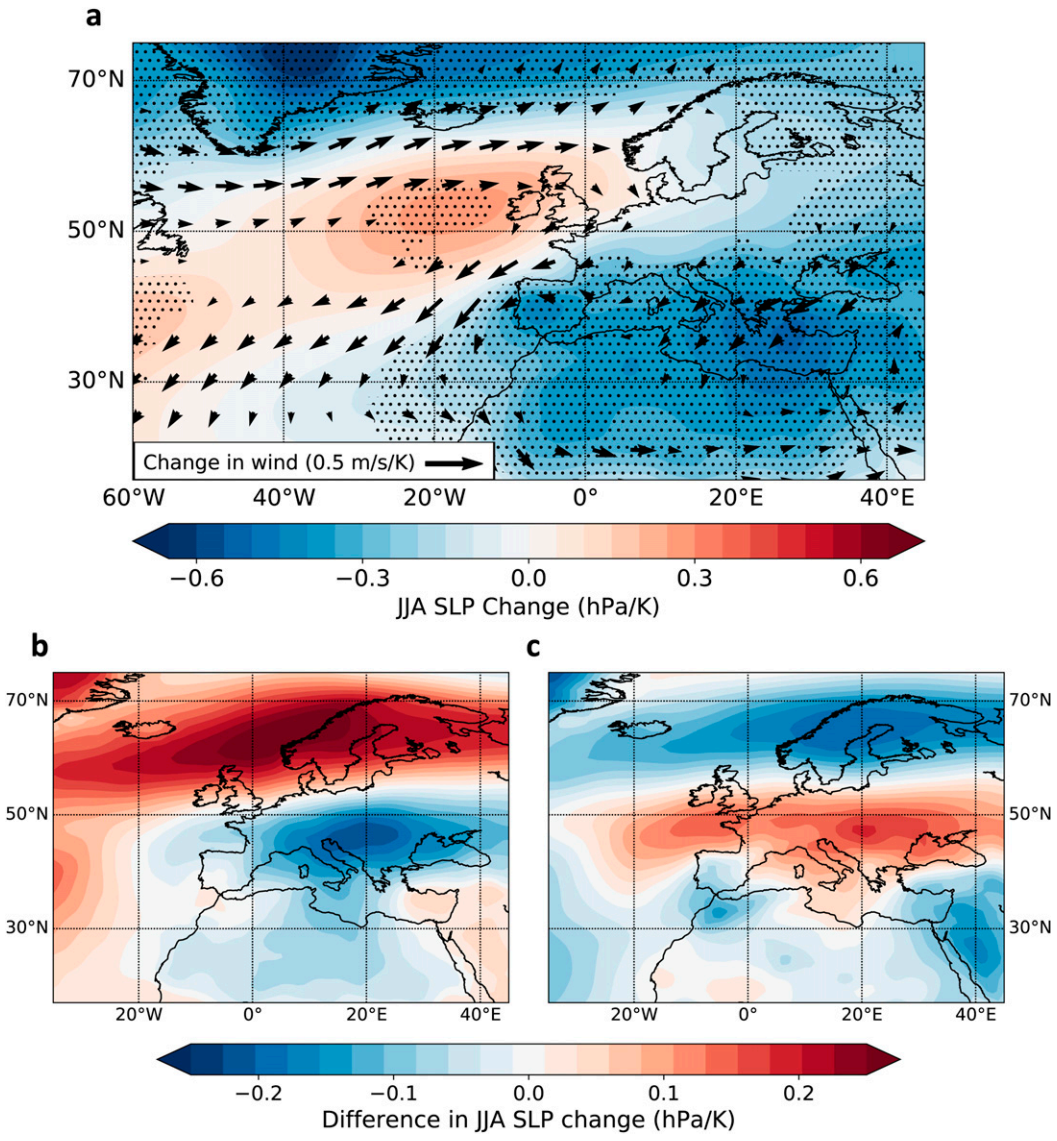

FIG. 11. (a) CMIP5 multimodel mean change (2071–2100 minus 1976–2005) in JJA SLP (shaded) and 850-hPa winds (arrows), normalized by each model's global-mean projected temperature change. Stippling indicates agreement on the sign of the change by at least 80% of models. Also shown is the difference in JJA SLP change relative to the CMIP5 multimodel mean for the six models with the most (b) negative and (c) positive moisture flux change (Fig. 9b).

low that results from enhanced surface warming in southern Europe. Yet, unlike Seager et al. (2014), and in agreement with Boé et al. (2009), we find that the influence of summer dynamics is largely confined northward of 45°N. South of that latitude, soil moisture–precipitation feedbacks, triggered by winter and spring drying, are dominant (Rowell and Jones 2006; Boé and Terray 2014). These mechanisms are also consistent with analyses of interannual variability in the summer storm track over northern Europe (Dong et al. 2013), as well as of spring precipitation and its link to summer temperatures (Vautard et al. 2007; Wang et al. 2011). Still, additional research is needed to quantify the respective importance and magnitude of the various physical mechanisms causing the summer drying. Such an analysis should rely on a common modeling framework with carefully designed experiments to investigate the effects of winter/spring precipitation anomalies or summer circulation changes. It would be critical in order to determine the effects of uncertainties in the magnitude of these physical drivers on future summer climate trends.

a. Mechanisms of spring circulation change

On its own, the dynamical adjustment approach we adopted in section 4c only highlights the consistency between large-scale, upper-tropospheric circulation changes and SLP trends over the Mediterranean. Assuming the future upper-tropospheric pattern as given, the near-surface response (winds and SLP) can be understood through the prism of the external mode, the dominant mode of variability in the vertical structure of the seasonal-mean circulation in the midlatitudes (Tuel et al. 2021b). The enhanced

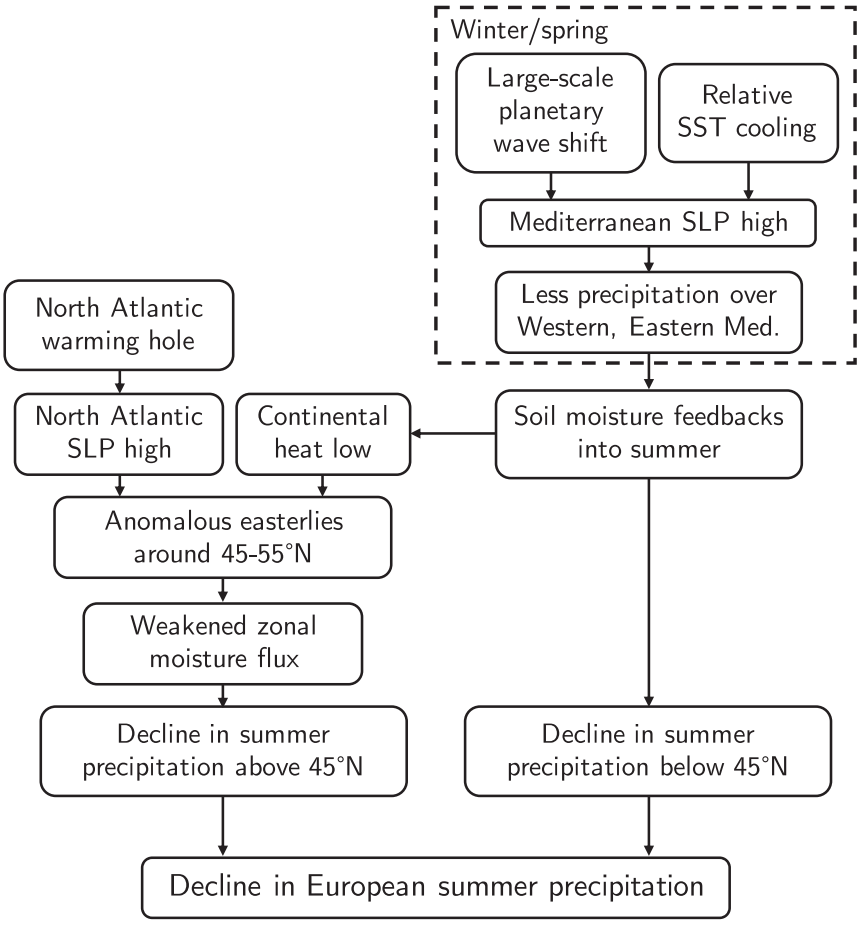

FIG. 12. Summary of physical mechanisms explaining the projected summer European drying.

near-surface response over the Mediterranean is caused by low vertical shear, as this region lies in the exit region of the North Atlantic storm track. Yet, the question remains as to what mechanisms are responsible for future upper-tropospheric circulation trends. Their similarity to winter changes suggests that mechanisms identified for winter still hold, such as a lengthening of the stationary wavelengths for planetary waves following the strengthening of the subtropical jet (Simpson et al. 2016). However, changes in the stratospheric vortex, for example, could also modulate the response (Zappa 2019). A detailed analysis of intermodel uncertainty in either winter or spring upper-tropospheric circulation trends is also still lacking (Sandler and Harnik 2020). The Mediterranean-scale circulation response to SST trends may also feed back onto the large-scale circulation, contributing to the trends projected by the GCMs. We cannot capture this effect in RCM simulations, since boundary conditions cannot be affected by perturbations within the domain. A global climate model would be required to investigate this point further.

b. *Soil moisture–precipitation feedbacks*

The notable sensitivity of summer climate in the southern half of the European domain to cold-season $P - E$ is consistent with previous results. Transitional regions between arid and wet climates are generally known to be hot spots of land–atmosphere coupling (Seneviratne et al. 2010; Orth and Seneviratne 2017). At the European scale, the analysis by Knist et al. (2017) based on the EURO-CORDEX model ensemble also confirmed that southern Europe was characterized by strong land–atmosphere coupling, unlike northern Europe. Evidence was found that interannual variability in winter and spring soil moisture in southern Europe impacted summer precipitation (Vautard et al. 2007) and the likelihood of summer hot days (Quesada et al. 2012; Mueller and Seneviratne 2012). For precipitation, the link may emerge not so much from the direct input of moisture to the atmosphere by evaporation from wet soils as from the impact that higher absolute humidity has on lower troposphere stability (Eltahir 1998; Seneviratne et al. 2010). Downstream precipitation of evaporated soil moisture may still matter locally, however. Soil moisture–precipitation feedbacks thus offer a physically based causal interpretation of the correlation results from Figs. 3 and 4. This causality could potentially be called into question if cold-season $P - E$ and summer climate were both impacted by a third, independent process, for instance a persistence in atmospheric dynamics or SSTs that would lead to larger-than-average precipitation from winter to summer. There is however no clear evidence for such a

process. The large contribution of surface evaporation to the summertime European moisture budget supports the idea that the correlation is linked to soil moisture–precipitation feedbacks. Simulations in which spring and summer soil moisture are set to a baseline value (and thus decoupled from cold-season $P - E$ variability) could help shed more light on this point.

Results from section 4 suggest that land–atmosphere coupling also explains much of the projected summer P decline in the southern part of our domain. There, the projected summer decline in E and soil moisture, and the weak $P - E$ trends (Fig. 5), are consistent with soil moisture–precipitation feedbacks being responsible for the concurrent P decline. Summer E notably decreases most over the Iberian Peninsula and the Balkans, the regions of our domain that experience the most severe P, $P - E$, and soil moisture declines during the cold season. These are also regions with notable land–atmosphere coupling in the present-day climate, that is, where summer E and low-level RH are most constrained by late spring soil moisture and winter/spring $P - E$ (Figs. 3e and 4). Notably, over the Iberian Peninsula (and northwestern Africa, outside of our domain), E is even projected to decline during MAM. This suggests that soil moisture constraints on E will in the future already be felt during spring, and that soil moisture depletion will occur earlier in the year.

By contrast, the fact that, over the northern half of the domain, summer E remains constant in future projections (Fig. 5f), despite lower P and soil moisture, is evidence that soil moisture feedbacks play a limited role there. Water saturation at the surface decreases, but likely remains high enough, combined with the enhanced evaporative demand in a warmer and drier climate, to maintain E at its historical value. The $P - E$ decline is driven by the decline in P. Future summer $P - E$ becomes clearly negative (as opposed to a historical value close to 0; Fig. 3a), a change sustained by enhanced depletion of soil moisture. This suggests that land–atmosphere coupling will strengthen over the northern half of the domain, as summer climate becomes increasingly reliant on cold-season accumulated soil moisture.

Still, it should be noted that CMIP5 GCMs may overestimate the strength of soil moisture–precipitation feedbacks due to their coarse resolution (Hohenegger et al. 2009). Biases in cloud parameterization or in the effect of anthropogenic aerosols in GCMs could also matter, and explain in particular why regional simulations may exhibit weaker warming and drying trends than their driving GCMs (Boé et al. 2020a).

c. Future trends in summer circulation

Section 5 showed that future summer circulation trends strongly constrained changes in zonal moisture advection, thus impacting the future European domain moisture budget.

First, positive SLP anomalies over the North Atlantic are thought to result from the weak SST warming trends in the region, also known as the North Atlantic warming hole (NAWH). The NAWH is believed to follow from a slowdown of the Atlantic meridional overturning circulation, although other forcings are not to be excluded (Hu and Fedorov 2020). Numerical simulations in which global climate models were forced with negative SST anomalies mimicking the NAWH exhibited an SLP response generally consistent in pattern and magnitude with the projected CMIP5 multimodel average (Fig. 11a) (Haarsma et al. 2015; Gervais et al. 2019). Still, the SLP response to the NAWH has only been analyzed in single-GCM experiments with one NAWH-like SST anomaly pattern only. Consequently, we still do not know what fraction of the spread in SLP trends across CMIP5 GCMs could be related to differences in NAWH trends themselves, or in the response to the NAWH itself. This is all the more difficult to determine as the NAWH SLP response resembles the positive phase of the summer NAO, changes in which also influence mean JJA SLP (Bladé et al. 2012). In particular, it remains unclear why some GCMs would project SLP increases over Scandinavia (Fig. 11b).

Second, negative SLP trends over the Mediterranean region have been shown to result from a heat low phenomenon: as the intense surface warming, caused by the decrease in summer precipitation, extends into the lower troposphere, it triggers an overall cyclonic anomaly around the area (Haarsma et al. 2009). This is in sharp contrast with winter and spring trends (Fig. 6a; see also Fig. S3a). Indeed, land surface warming around the Mediterranean is by far largest during summer (Lionello and Scarascia 2018). In addition, near-surface static stability over land is lowest during summer (Fig. S5), thus favoring the upward propagation of the surface warming and the associated circulation response. By contrast, in winter, near-surface static stability is large over land, but low over the Mediterranean Sea. This explains why the relative SST cooling spreads upward into the lower troposphere during winter only, generating an anomalous SLP ridge (Tuel et al. 2021b).

d. Summer RH and precipitation

Our focus here has been primarily on moisture fluxes and near-surface RH, instead of precipitation. This is in part physically motivated (e.g., since dynamics act on precipitation through their effect on the moisture budget) but is also because CMIP5 models are known to differ widely in their representation of feedbacks between atmospheric humidity, clouds, and surface processes. Indeed, differences in the representation of land–atmosphere coupling, notably cloud feedbacks, were found to be related to uncertainties in projections of summer precipitation across global and regional climate models (Boé and Terray 2014), with evidence pointing toward noticeable model deficiencies likely impacting future projections (Boberg and Christensen 2012; Orth et al. 2016; Boé et al. 2020a,b). This added uncertainty might therefore complicate the analysis of intermodel scatter. We show in Fig. 13a interannual variability in summer precipitation and 850-hPa RH across observational, reanalysis, and CMIP5 data. It is striking to observe that the CMIP5 models neatly divide themselves into two groups with similar precipitation–RH relationships, one consistent with ERA5 and various precipitation datasets and the other not. In addition, CMIP5 models vary widely in their mean summer climate, in particular in average 850-hPa RH. This matters because the precipitation–RH relationship is not linear, precipitation being less sensitive to RH variability as mean RH decreases (Fig. 13a). This leads to poor correlation between JJA RH and precipitation changes in CMIP5 projections

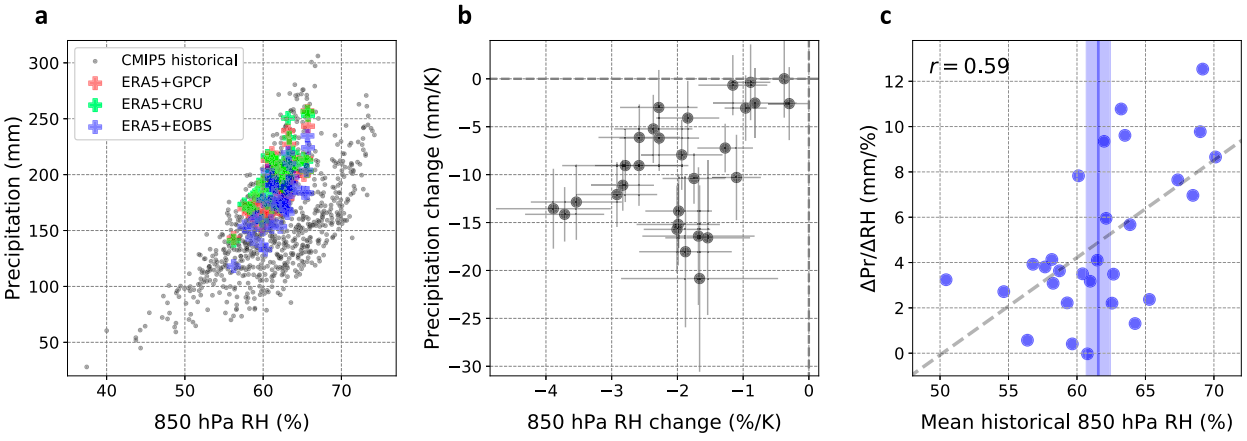

FIG. 13. (a) Interannual variability in JJA European (10°W–30°E, 30°–50°N) 850-hPa RH and precipitation: output from CMIP5 models (1976–2005; black), and data from ERA5 (for RH) and GPCP (red), CRU TS4 (green), and EOBS (blue) (for precipitation). (b) Change in JJA European precipitation against change in 850-hPa RH across CMIP5 models. 95% confidence intervals are shown by light gray lines. (c) Sensitivity of projected JJA precipitation change to RH change across CMIP5 models, against mean historical JJA European RH. The ERA5 mean summer RH is shown by the thick vertical blue line, along with its 95% confidence interval.

(Fig. 13b). The nonuniqueness of the relationship stands in contrast to other seasons, when the share of convective precipitation is lower, and dynamics matter more than model parameterizations. Consistent with Fig. 13a, mean historical RH provides a useful constraint on the sensitivity of mean precipitation to changes in background RH (Fig. 13c). ERA5 indicates a mean RH value of 61%–62% over Europe during summer, which falls roughly along the CMIP5 median. This adds further uncertainty to future precipitation trends, since for the same RH change, different models may project widely different P changes. In particular, some models may be less reliable for precipitation projections because they are too sensitive to variations in low-level RH.

7. Conclusions

The broad division of continental Europe into a southern region, which is dependent on evaporation of cold-season water storage to maintain summer atmospheric humidity, and a northern region, which is reliant on the narrow North Atlantic moisture jet, emerges from the analysis of historical summertime moisture fluxes. This dichotomy, though imperfect, is useful to understand future summer projections over the European domain. Since evapotranspiration is a primary source of moisture south of 45°N, the region is logically highly sensitive to variations in the winter/spring moisture budget. It is led toward robust drying, dictated by soil moisture–precipitation feedbacks, as cold-season precipitation declines, due to changes in regional circulation caused by shifts in planetary waves and a relative cooling of Mediterranean SSTs compared to land. Those feedbacks also lead to enhanced summer warming and to the development of a Mediterranean-wide heat low that contributes to weakening the incoming moisture transport toward northwestern Europe upon which this last region depends on to maintain its moisture during summer. In parallel, a large-scale land–ocean warming contrast over the North Atlantic, enhanced by the weakening of the AMOC, is followed by the development of anomalous anticyclonic circulation west of the British Isles, which also acts to reduce the westerly transport of moisture toward the continent.

While some of the various physical mechanisms presented here have been previously discussed, this study has sought to provide a comprehensive, physical picture of summer European drying, and to describe how these different mechanisms interact with each other. We also anchored summer climate change over southern Europe into a physical understanding of cold-season precipitation trends. Several major sources of uncertainty were discussed, including moisture flux projections and the sensitivity of regional precipitation to RH. The adoption of a common modeling framework may help to better assess the respective role of these various mechanisms in future summer climate trends.

Acknowledgments. We acknowledge the World Climate Research Programme's Working Group on Coupled Modelling, which is responsible for CMIP, and we thank the climate modeling groups for producing and making available their model output. This work was funded by the Office Chérifien des Phosphates (OCP) through the Université Mohamed VI Polytechnique, Morocco.

Data availability statement. ERA5 reanalysis data are available from 1979 to 2019 and can be downloaded from https://cds.climate.copernicus.eu/cdsapp#!/dataset/reanalysis-era5-pressure-levels?tab=overview. CMIP5 model output were downloaded from https://esgf-index1.ceda.ac.uk/projects/esgf-ceda/. Regional simulations are available on request from the corresponding author.

REFERENCES

Adler, R. F., and Coauthors, 2003: The version-2 Global Precipitation Climatology Project (GPCP) monthly precipitation analysis (1979–present). *J. Hydrometeor.*, **4**, 1147–1167, https://doi.org/10.1175/1525-7541(2003)004<1147:TVGPCP>2.0.CO;2.

Bador, M., L. Terray, and J. Boé, 2016: Emergence of human influence on summer record–breaking temperatures over Europe. *Geophys. Res. Lett.*, **43**, 404–412, https://doi.org/10.1002/2015GL066560.

Belleflamme, A., X. Fettweis, and M. Erpicum, 2015: Do global warming–induced circulation pattern changes affect temperature and precipitation over Europe during summer? *Int. J. Climatol.*, **35**, 1484–1499, https://doi.org/10.1002/joc.4070.

Bladé, I., D. Fortuny, G. J. van Oldenborgh, and B. Liebmann, 2012: The summer North Atlantic Oscillation in CMIP3 models and related uncertainties in projected summer drying in Europe. *J. Geophys. Res. Atmos.*, **117**, D16104, https://doi.org/10.1029/2012JD017816.

Boberg, F., and J. H. Christensen, 2012: Overestimation of Mediterranean summer temperature projections due to model deficiencies. *Nat. Climate Change*, **2**, 433–436, https://doi.org/10.1038/nclimate1454.

Boé, J., and L. Terray, 2014: Land–sea contrast, soil-atmosphere and cloud-temperature interactions: Interplays and roles in future summer European climate change. *Climate Dyn.*, **42**, 683–699, https://doi.org/10.1007/s00382-013-1868-8.

——, ——, C. Cassou, and J. Najac, 2009: Uncertainties in European summer precipitation changes: Role of large scale circulation. *Climate Dyn.*, **33**, 265–276, https://doi.org/10.1007/s00382-008-0474-7.

——, S. Somot, L. Corre, and P. Nabat, 2020a: Large discrepancies in summer climate change over Europe as projected by global and regional climate models: Causes and consequences. *Climate Dyn.*, **54**, 2981–3002, https://doi.org/10.1007/s00382-020-05153-1.

——, and Coauthors, 2020b: Past long-term summer warming over western Europe in new generation climate models: Role of large-scale atmospheric circulation. *Environ. Res. Lett.*, **15**, 084038, https://doi.org/10.1088/1748-9326/ab8a89.

Brogli, R., S. L. Sørland, N. Kröner, and C. Schär, 2019: Causes of future Mediterranean precipitation decline depend on the season. *Environ. Res. Lett.*, **14**, 114017, https://doi.org/10.1088/1748-9326/ab4438.

Byrne, M. P., and P. A. O'Gorman, 2018: Trends in continental temperature and humidity directly linked to ocean warming. *Proc. Natl. Acad. Sci. USA*, **115**, 4863–4868, https://doi.org/10.1073/pnas.1722312115.

Cornes, R. C., G. van der Schrier, E. J. M. van den Besselaar, and P. D. Jones, 2018: An ensemble version of the E-OBS temperature and precipitation data sets. *J. Geophys. Res. Atmos.*, **123**, 9391–9409, https://doi.org/10.1029/2017JD028200.

Dong, B., R. T. Sutton, T. Woollings, and K. Hodges, 2013: Variability of the North Atlantic summer storm track: Mechanisms and impacts on European climate. *Environ. Res. Lett.*, **8**, 034037, https://doi.org/10.1088/1748-9326/8/3/034037.

Eltahir, E. A. B., 1998: A soil moisture–rainfall feedback mechanism: 1. Theory and observations. *Water Resour. Res.*, **34**, 765–776, https://doi.org/10.1029/97WR03499.

Fischer, E. M., S. I. Seneviratne, P. L. Vidale, D. Lüthi, and C. Schär, 2007: Soil moisture–atmosphere interactions during the 2003 European summer heat wave. *J. Climate*, **20**, 5081–5099, https://doi.org/10.1175/JCLI4288.1.

Gervais, M., J. Shaman, and Y. Kushnir, 2019: Impacts of the North Atlantic warming hole in future climate projections: Mean atmospheric circulation and the North Atlantic jet. *J. Climate*, **32**, 2673–2689, https://doi.org/10.1175/JCLI-D-18-0647.1.

Grillakis, M. G., 2019: Increase in severe and extreme soil moisture droughts for Europe under climate change. *Sci. Total Environ.*, **660**, 1245–1255, https://doi.org/10.1016/j.scitotenv.2019.01.001.

Gruber, A., T. Scanlon, R. van der Schalie, W. Wagner, and W. Dorigo, 2019: Evolution of the ESA CCI soil moisture climate data records and their underlying merging methodology. *Earth Syst. Sci. Data*, **11**, 717–739, https://doi.org/10.5194/essd-11-717-2019.

Haarsma, R. J., F. Selten, B. van den Hurk, W. Hazeleger, and X. Wang, 2009: Drier Mediterranean soils due to greenhouse warming bring easterly winds over summertime central Europe. *Geophys. Res. Lett.*, **36**, L04705, https://doi.org/10.1029/2008GL036617.

——, ——, and S. S. Drijfhout, 2015: Decelerating Atlantic meridional overturning circulation main cause of future west European summer atmospheric circulation changes. *Environ. Res. Lett.*, **10**, 094007, https://doi.org/10.1088/1748-9326/10/9/094007.

Harris, I., T. J. Osborn, P. Jones, and D. Lister, 2020: Version 4 of the CRU TS monthly high-resolution gridded multivariate climate dataset. *Sci. Data*, **7**, 109, https://doi.org/10.1038/s41597-020-0453-3.

Hersbach, H., and Coauthors, 2020: The ERA5 global reanalysis. *Quart. J. Roy. Meteor. Soc.*, **146**, 1999–2049, https://doi.org/10.1002/qj.3803.

Hohenegger, C., P. Brockhaus, C. S. Bretherton, and C. Schär, 2009: The soil moisture–precipitation feedback in simulations with explicit and parameterized convection. *J. Climate*, **22**, 5003–5020, https://doi.org/10.1175/2009JCLI2604.1.

Hu, S., and A. V. Fedorov, 2020: Indian Ocean warming as a driver of the North Atlantic warming hole. *Nat. Commun.*, **11**, 4785, https://doi.org/10.1038/s41467-020-18522-5.

Im, E. S., R. L. Gianotti, and E. A. B. Eltahir, 2014: Improving the simulation of the West African monsoon using the MIT regional climate model. *J. Climate*, **27**, 2209–2229, https://doi.org/10.1175/JCLI-D-13-00188.1.

Kew, S., S. Y. Philip, G. Jan van Oldenborgh, G. van der Schrier, F. E. L. Otto, and R. Vautard, 2019: The exceptional summer heat wave in southern Europe 2017. *Bull. Amer. Meteor. Soc.*, **100** (1), S49–S53, https://doi.org/10.1175/BAMS-D-18-0109.1.

Knist, S., and Coauthors, 2017: Land–atmosphere coupling in EURO-CORDEX evaluation experiments. *J. Geophys. Res. Atmos.*, **122**, 79–103, https://doi.org/10.1002/2016JD025476.

Lionello, P., and L. Scarascia, 2018: The relation between climate change in the Mediterranean region and global warming. *Reg. Environ. Change*, **18**, 1481–1493, https://doi.org/10.1007/s10113-018-1290-1.

Mueller, B., and S. I. Seneviratne, 2012: Hot days induced by precipitation deficits at the global scale. *Proc. Natl. Acad. Sci. USA*, **109**, 12 398–12 403, https://doi.org/10.1073/pnas.1204330109.

Orth, R., and S. I. Seneviratne, 2017: Variability of soil moisture and sea surface temperatures similarly important for warm-season land climate in the Community Earth System Model. *J. Climate*, **30**, 2141–2162, https://doi.org/10.1175/JCLI-D-15-0567.1.

——, J. Zscheischler, and S. I. Seneviratne, 2016: Record dry summer in 2015 challenges precipitation projections in Central Europe. *Sci. Rep.*, **6**, 28334, https://doi.org/10.1038/srep28334.

Pal, J. S., and Coauthors, 2007: Regional climate modeling for the developing world: The ICTP RegCM3 and RegCNET. *Bull. Amer. Meteor. Soc.*, **88**, 1395–1410, https://doi.org/10.1175/BAMS-88-9-1395.

Quesada, B., R. Vautard, P. Yiou, M. Hirschi, and S. I. Seneviratne, 2012: Asymmetric European summer heat predictability from

wet and dry southern winters and springs. *Nat. Climate Change*, **2**, 736–741, https://doi.org/10.1038/nclimate1536.

Rodwell, M. J., and B. J. Hoskins, 2001: Subtropical anticyclones and summer monsoons. *J. Climate*, **14**, 3192–3211, https://doi.org/10.1175/1520-0442(2001)014<3192:SAASM>2.0.CO;2.

Rowell, D. P., and R. G. Jones, 2006: Causes and uncertainty of future summer drying over Europe. *Climate Dyn.*, **27**, 281–299, https://doi.org/10.1007/s00382-006-0125-9.

Samaniego, L., and Coauthors, 2018: Anthropogenic warming exacerbates European soil moisture droughts. *Nat. Climate Change*, **8**, 421–426, https://doi.org/10.1038/s41558-018-0138-5.

Sandler, D., and N. Harnik, 2020: Future wintertime meridional wind trends through the lens of subseasonal teleconnections. *Wea. Climate Dyn.*, **1**, 427–443, https://doi.org/10.5194/wcd-1-427-2020.

Schär, C., P. L. Vidale, D. Lüthi, C. Frei, C. Häberli, M. A. Liniger, and C. Appenzeller, 2004: The role of increasing temperature variability in European summer heatwaves. *Nature*, **427**, 332–336, https://doi.org/10.1038/nature02300.

Seager, R., H. Liu, N. Henderson, I. R. Simpson, C. Kelley, T. Shaw, Y. Kushnir, and M. Ting, 2014: Causes of increasing aridification of the Mediterranean region in response to rising greenhouse gases. *J. Climate*, **27**, 4655–4676, https://doi.org/10.1175/JCLI-D-13-00446.1.

Seneviratne, S. I., D. Lüthi, M. Litschi, and C. Schär, 2006: Land–atmosphere coupling and climate change in Europe. *Nature*, **443**, 205–209, https://doi.org/10.1038/nature05095.

——, T. Corti, E. L. Davin, M. Hirschi, E. B. Jaeger, I. Lehner, B. Orlowsky, and A. J. Teuling, 2010: Investigating soil moisture–climate interactions in a changing climate: A review. *Earth-Sci. Rev.*, **99**, 125–161, https://doi.org/10.1016/j.earscirev.2010.02.004.

Simpson, I. R., R. Seager, M. Ting, and T. A. Shaw, 2016: Causes of change in Northern Hemisphere winter meridional winds and regional hydroclimate. *Nat. Climate Change*, **6**, 65–70, https://doi.org/10.1038/nclimate2783.

Stott, P. A., D. A. Stone, and M. R. Allen, 2004: Human contribution to the European heatwave of 2003. *Nature*, **432**, 610–614, https://doi.org/10.1038/nature03089.

Sutton, R. T., B. Dong, and J. M. Gregory, 2007: Land/sea warming ratio in response to climate change: IPCC AR4 model results and comparison with observations. *Geophys. Res. Lett.*, **34**, L02701, https://doi.org/10.1029/2006GL028164.

Taylor, K. E., R. J. Stouffer, and G. A. Meehl, 2012: An overview of CMIP5 and the experiment design. *Bull. Amer. Meteor. Soc.*, **93**, 485–498, https://doi.org/10.1175/BAMS-D-11-00094.1.

Tuel, A., and E. A. B. Eltahir, 2020: Why is the Mediterranean a climate change hot spot? *J. Climate*, **33**, 5829–5843, https://doi.org/10.1175/JCLI-D-19-0910.1.

——, S. Kang, and E. A. B. Eltahir, 2021a: Understanding climate change over the southwestern Mediterranean using high-resolution simulations. *Climate Dyn.*, **56**, 985–1001, https://doi.org/10.1007/s00382-020-05516-8.

——, P. A. O'Gorman, and E. A. B. Eltahir, 2021b: Elements of the dynamical response to climate change over the Mediterranean. *J. Climate*, **34**, 1135–1146, https://doi.org/10.1175/JCLI-D-20-0429.1.

Vautard, R., and Coauthors, 2007: Summertime European heat and drought waves induced by wintertime Mediterranean rainfall deficit. *Geophys. Res. Lett.*, **34**, L07711, https://doi.org/10.1029/2006GL028001.

——, and Coauthors, 2020: Human contribution to the record-breaking June and July 2019 heatwaves in Western Europe. *Environ. Res. Lett.*, **15**, 094077, https://doi.org/10.1088/1748-9326/aba3d4.

Wang, G., A. J. Dolman, and A. Alessandri, 2011: A summer climate regime over Europe modulated by the North Atlantic Oscillation. *Hydrol. Earth Syst. Sci.*, **15**, 57–64, https://doi.org/10.5194/hess-15-57-2011.

Wilks, D. S., 2016: "The stippling shows statistically significant grid points": How research results are routinely overstated and overinterpreted, and what to do about it. *Bull. Amer. Meteor. Soc.*, **97**, 2263–2273, https://doi.org/10.1175/BAMS-D-15-00267.1.

Wills, R. C., R. H. White, and X. J. Levine, 2019: Northern Hemisphere stationary waves in a changing climate. *Curr. Climate Change Rep.*, **5**, 372–389, https://doi.org/10.1007/s40641-019-00147-6.

Zappa, G., 2019: Regional climate impacts of future changes in the mid-latitude atmospheric circulation: A storyline view. *Curr. Climate Change Rep.*, **5**, 358–371, https://doi.org/10.1007/s40641-019-00146-7.